Crystal and magnetic structure of antiferromagnetic HoAuGe

2001 J. Phys.: Condens. Matter 13 2593

(http://iopscience.iop.org/0953-8984/13/11/315)

INSTITUTE OF PHYSICS PUBLISHING JOURNAL OF PHYSICS: CONDENSED MATTER

J. Phys.: Condens. Matter **13** (2001) 2593–2606 www.iop.org/Journals/cm PII: S0953-8984(01)17267-X

Crystal and magnetic structure of antiferromagnetic HoAuGe

B J Gibson[1,5], R Pöttgen[2], W Schnelle[3], B Ouladdiaf[4] and R K Kremer[1]

[1] Max-Planck-Institut für Festkörperforschung, Heisenbergstraße 1, D-70569 Stuttgart, Germany
[2] Department für Chemie, Butenandtstraße 5–13, Ludwig-Maximillians-Universität, D-81377 München-Grosshadern, Germany
[3] Max-Planck-Institut für Chemische Physik fester Stoffe, Pirnaer Landstaße 176, D-01257 Dresden, Germany
[4] Institut Laue–Langevin, Avenue des Martyrs, BP 156, F-38042 Grenoble, France

Received 19 September 2000, in final form 30 January 2001

Abstract

HoAuGe was prepared from the elements by arc melting and subsequent annealing at 1070 K. Its crystal structure was refined from single-crystal x-ray diffractometer data: $a = 440.10(5)$ pm, $c = 723.26(9)$ pm, $V = 0.1213(1)$ nm^3, $wR2 = 0.0640$, 225 F^2-values and ten variables. The nuclear structure was confirmed by neutron powder diffraction. HoAuGe adopts the NdPtSb-type structure. The gold and germanium atoms form two-dimensional infinite [AuGe] polyanions with intralayer Au–Ge distances of 260.5 pm, while the interlayer Au–Ge distances of 304.1 pm are much longer. The polyanions are separated by the holmium ions. Magnetic susceptibility, specific heat capacity and neutron diffraction measurements reveal antiferromagnetic ordering at $T_N = 5.6(2)$ K with further magnetic reordering at $T_1 = 3.5(2)$ K and $T_2 = 2.4(2)$ K. At higher temperatures Curie–Weiss behaviour is observed with $\mu_{eff}^{exp} = 10.2(2)\ \mu_B$ and $\Theta_p = 0(1)$ K. From the magnetic specific heat a fourfold-degenerate ground state is found. The magnetic structure at 1.3 K is described by the propagation vector $\vec{k} = (1/2, 0, 0)$ with the Ho spins oriented within the *bc*-plane. As the temperature increases towards T_N, the magnetic structure becomes incommensurate, which accounts for the observed additional transitions below T_N.

1. Introduction

During the last few years we have intensively investigated the crystal structures, electronic structures and physical properties of several rare-earth-metal–gold germanides, REAuGe (RE = Sc, Y, La, Ce, Gd, Lu) [1–5]. The crystal structures of these compounds are derived from the $CaIn_2$ type by an ordered arrangement of the gold and germanium atoms at the indium position. While the germanides with the large rare-earth atoms may be ascribed to the NdPtSb

[5] Author to whom any correspondence should be addressed.

0953-8984/01/112593+14$30.00

branch of the ordered $CaIn_2$ structure, those with the smaller ones belong to the LiGaGe branch. An exception is EuAuGe [6], which adopts its own structure type owing to the divalent state of the europium [7].

We have now extended our investigations to the compounds with magnetic rare-earth atoms. A study of the magnetic properties arising in these compounds is of interest due to the wide variety of magnetic phenomena that are frequently observed in RE–intermetallic compounds. Long-range magnetic ordering (often of a complex nature) is usually found due to the localized character of the 4f electrons. Strong hybridization of the 4f electrons with the conduction band may lead to more exotic phenomena such as heavy-fermion behaviour, the Kondo effect or superconductivity [8].

In the present paper we report in detail on the magnetic properties and structure as well as on electrical resistivity and heat capacity measurements of HoAuGe. Preliminary results of some of this work have been published previously [9].

2. Experimental procedure

The starting materials for the preparation of HoAuGe were ingots of holmium (Johnson-Matthey), gold wire (Degussa) and germanium lumps (Wacker) all with stated purity better than 99.9%. The holmium ingots were cut into small pieces and arc melted under argon to buttons of about 500 mg in a first step. The argon was previously purified by molecular sieves, a titanium sponge (at 900 K) and an oxisorb catalyst [10]. The holmium buttons were subsequently mixed with the gold wire and the germanium lumps in the ideal 1:1:1 atomic ratio, and the samples prepared by arc melting in a miniaturized arc-melting apparatus [11]. The melted buttons were turned over and each side was remelted three times to ensure homogeneity. The weight loss after several meltings was always smaller than 0.2%. The buttons were subsequently enclosed in evacuated quartz glass tubes and annealed at 1070 K for ten days. They are light grey with metallic lustre, stable in air and quite brittle. No visible decomposition was observed, even after a period of exposure to air of several months.

In order to check the purity of our products, all samples were characterized through their x-ray powder diagrams using the modified Guinier technique [12] with Cu $K\alpha_1$ radiation and silicon ($a = 543.07$ pm) as an internal standard. All powder patterns showed single-phase samples. The lattice constants (see table 1) were refined from the powder data by least-squares fits. To assure correct indexing, the observed patterns were compared to calculated ones [13], taking the atomic parameters from the structure refinement. Our lattice constants (see table 1) are in excellent agreement with the powder data given earlier by Rossi *et al* [14].

Single-crystal intensity data were measured at room temperature using a four-circle diffractometer (Enraf-Nonius CAD4) with graphite-monochromatized Mo $K\alpha$ radiation ($\lambda = 71.073$ pm) and a scintillation counter with pulse-height discrimination. An empirical absorption correction was applied on the basis of psi scan data.

Magnetic susceptibilities were measured on a polycrystalline block of $\approx$70 mg using a SQUID magnetometer (MPMS, Quantum Design) between 2 and 300 K, and at magnetic flux densities up to 5.5 T.

The electrical resistivity measurement was performed on a small bar ($\approx 3.0 \times 2.5 \times 2.0$ mm^3, cut with a diamond saw from the polycrystalline ingots) with a conventional dc four-probe technique in the temperature range 4.2 K to 300 K. Cooling and heating curves taken at a constant current were identical within error bars.

The sample for heat capacity measurement was polished on one face and mounted on the sapphire sample holder of the calorimeter with a minute amount of vacuum grease (Apiezon N). The addenda heat capacity was measured separately and subtracted. We

Table 1. Crystal data and structure refinement for HoAuGe.

Empirical formula	HoAuGe
Formula weight	434.49 g mol^{-1}
Crystal system, space group	Hexagonal, $P6_3mc$
Unit-cell dimensions	$a = 440.10(5)$ pm
(Guinier powder data)	$c = 723.26(9)$ pm
	$V = 0.1213(1)$ nm^3
Formula units per cell	$Z = 2$
Calculated density	11.89 g cm^{-3}
Crystal size	$40 \times 40 \times 40$ μm^3
Transmission ratio (max:min)	4.07
Absorption coefficient	104.5 mm^{-1}
$F(000)$	356
θ-range for data collection	5° to 30°
Scan type	$\omega/2\theta$
Range in hkl	±7, ±7, ±13
Total No of reflections	973
Independent reflections	234 ($R_{\rm int} = 0.0879$)
Reflections with $I > 2\sigma(I)$	208 ($R_\sigma = 0.0539$)
Refinement method	Full-matrix least-squares method on F^2
Data/restraints/parameters	225/0/10
Goodness of fit on F^2	1.111
Final R-indices ($I > 2\sigma(I)$)	$R_1 = 0.0316$, $wR2 = 0.0610$
R-indices (all data)	$R_1 = 0.0366$, $wR2 = 0.0640$
Extinction coefficient	0.016(2)
Largest diffraction peak and hole	2562 and -2411 electrons nm^{-3}
Absolute structure parameter	0.08(4)

used the quasi-adiabatic step-heating method (Nernst's method) [15]. The inaccuracy of $c_p(T)$ is ≈1.5%.

The neutron powder diffraction data were collected on the high-flux two-axis diffractometer D1B [16] situated at the Institut Laue–Langevin. We used a wavelength of $\lambda = 252.2$ pm, emerging from a pyrolytic graphite (002) monochromator. Two sets of patterns were recorded at 1.3 K and 50 K over the range $6° < 2\theta < 86°$. Measurements at selected temperatures between these two extremes were subsequently recorded in order to examine the evolution of the magnetic structure as a function of temperature. Measurements were performed on a coarsely powdered sample of ≈8 g enclosed in a double-walled vanadium can in order to reduce the effects of absorption by ^{197}Au.

3. Results

3.1. Single-crystal x-ray diffraction

Single crystals of HoAuGe were selected from a crushed button after annealing and investigated by Buerger precession photographs in order to check their symmetry and suitability for intensity data collection. The systematic extinctions were compatible with the space groups $P6_3mc$, $P6_3/mmc$ and $P\bar{6}2c$, of which $P6_3mc$ was found to be correct in agreement with earlier investigations [1–3]. Crystallographic data and some details of the data collection are summarized in table 1. See also figure 1.

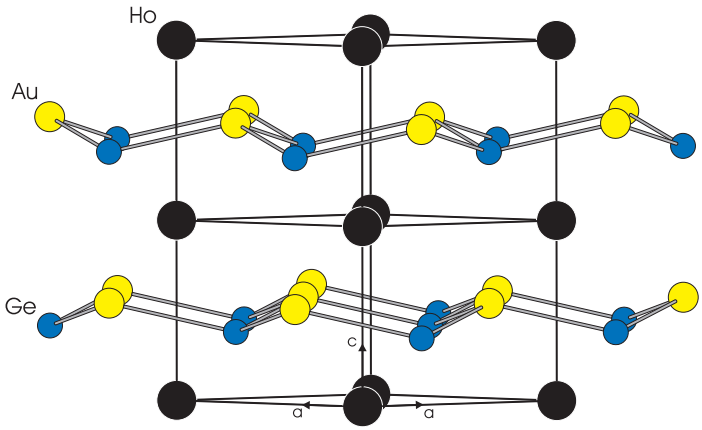

Figure 1. The crystal structure of HoAuGe.

The structure was refined using SHELXL-93 [17] with anisotropic displacement parameters for all atoms. Within the refinement, nine reflections with '$F_o^2 < -2\sigma(F_o^2)$' [17] were treated as unobserved. A final difference Fourier analysis did not indicate electron densities above the level of background noise. The highest residual peak (see table 1) was too small and too close to the gold position (89 pm) to be indicative for an additional atomic site. It most probably resulted from an incomplete absorption correction of the data. Atomic parameters and interatomic distances are listed in tables 2 and 3. Listings of the structure factors and the anisotropic displacement parameters are available[6].

Table 2. Atomic coordinates and isotropic displacement parameters (pm^2) for HoAuGe. U_{eq} is defined as one third of the trace of the orthogonalized U_{ij}-tensor.

Atom	Wyckoff site	x	y	z	U_{eq} (pm^2)
X-ray single-crystal data, 293 K					
$a = 440.10(5)$ pm, $c = 723.26(9)$ pm					
Ho	2a	0	0	0.9628(3)	69(2)
Au	2b	1/3	2/3	0.2500[a]	91(3)
Ge	2b	1/3	2/3	0.6705(5)	72(5)
Neutron powder data, 50 K					
$a = 440.2(1)$ pm, $c = 720.4(3)$ pm					
Ho	2a	0	0	0.963(1)	60
Au	2b	1/3	2/3	0.2500[a]	60
Ge	2b	1/3	2/3	0.670(1)	60

[a] Fixed parameter [19].

3.2. Magnetic susceptibility

The molar magnetic susceptibility $\chi_{mol}(T)$ of HoAuGe measured below $T = 50$ K and in an external field of $H_{ext} = 0.1$ T is plotted in figure 2. A sharp antiferromagnetic phase transition is observed at $T_N = 5.6(5)$ K. Below T_N, two additional anomalies are observed at $T_1 = 4(1)$ K

[6] Details may be obtained from the Fachinformationszentrum Karlsruhe, D-76344 Eggenstein-Leopoldshafen, Germany, by quoting the Registry No CSD-410822.

Table 3. Interatomic distances (pm) calculated with the powder lattice constants and the positional parameters of the single-crystal data in the structure of HoAuGe. All distances shorter than 565 pm (Ho–Ho), 525 pm (Ho–Au, Ho–Ge) and 415 pm (Au–Au, Au–Ge, Ge–Ge) are listed. The standard deviations are all equal to or smaller than 0.3 pm.

Ho :	3 Ge 295.2	Au :	3 Ge 260.5	Ge :	3 Au 260.5
	3 Au 297.1		3 Ho 297.1		3 Ho 295.2
	3 Au 328.2		1 Ge 304.1		1 Au 304.1
	3 Ge 330.6		3 Ho 328.2		3 Ho 330.6
	2 Ho 361.6				
	6 Ho 440.1				

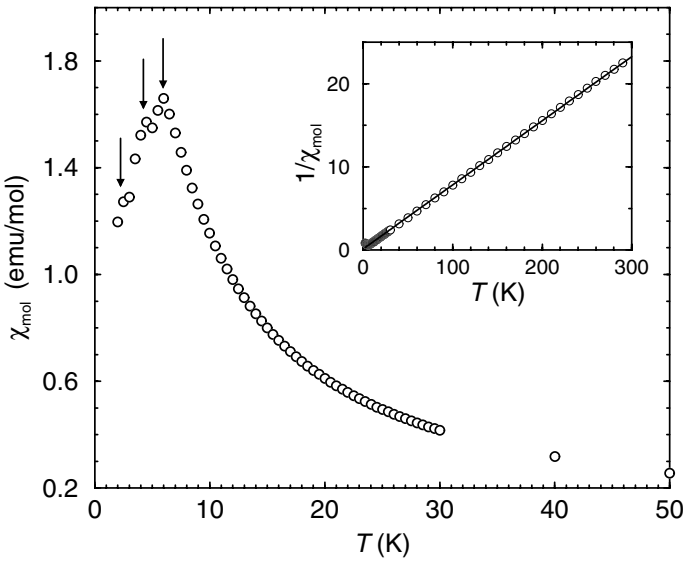

Figure 2. The low-temperature magnetic susceptibility of HoAuGe measured in an external field of $H_{\mathrm{ext}} = 0.1$ T. The inset shows the inverse magnetic susceptibility, with the solid line representing a fit to the Curie–Weiss law above $T = 20$ K.

and at $T_2 = 2(1)$ K. Although the resolution of this susceptibility measurement is insufficient to determine the nature of these anomalies, they are also observed in the heat capacity and neutron scattering measurements, which are discussed in more detail later.

Above $T \approx 20$ K, the magnetic susceptibility obeys the Curie–Weiss law $\chi_{\mathrm{mol}} = C/(T - \Theta_{\mathrm{p}})$ where Θ_{p} is the paramagnetic Curie temperature and C is the Curie constant. The high-temperature susceptibility is plotted as $1/\chi_{\mathrm{mol}}$ versus T in the inset of figure 2. This experimental curve is fitted above $T = 20$ K. The fit to the data results in a paramagnetic Curie temperature of $\Theta_{\mathrm{p}} = 0(1)$ K, and $\mu_{\mathrm{eff}}^{\mathrm{exp}} = 10.2(2)\ \mu_{\mathrm{B}}$. The value of $\mu_{\mathrm{eff}}^{\mathrm{exp}}$ is in close agreement with the value of $\mu_{\mathrm{eff}} = 10.6\ \mu_{\mathrm{B}}$ for free Ho^{3+} ions (ground-state configuration $^5I_8$).

The magnetic moment of HoAuGe is plotted as a function of external field for several isotherms below T_{N} in figure 3. A magnetic transition is observed at $H_{\mathrm{ext}} = 0.4$ T in the $T = 2$ K isotherm. The magnetic Ho ions nearly reach saturation in the maximum measured field of $H_{\mathrm{ext}} = 5.5$ T. At $H_{\mathrm{ext}} = 5.5$ T the magnetic moment, $m(H_{\mathrm{ext}})$, has a value of 7.2(2) μ_{B}/Ho atom which is significantly reduced from the corresponding value of $g_J J = 10\ \mu_{\mathrm{B}}$ that is calculated for free Ho^{3+}. This reduced Ho moment could be attributed to either CEF effects or to the magnetocrystalline anisotropy within the polycrystalline sample.

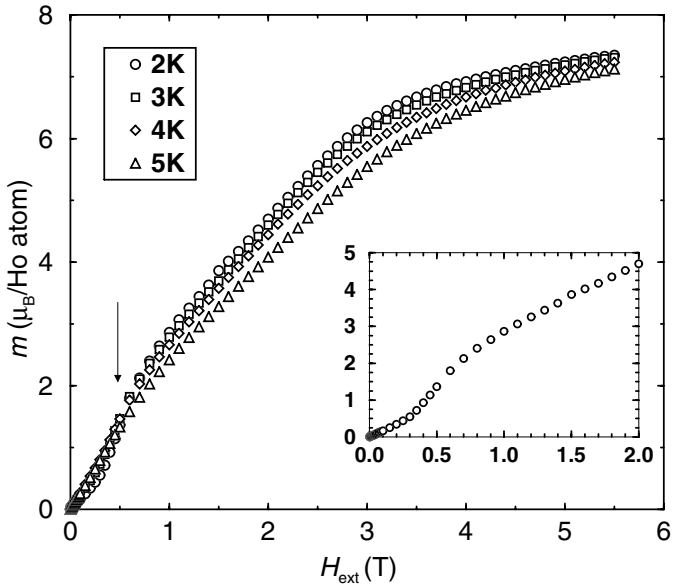

Figure 3. A selection of magnetization isotherms for HoAuGe taken at $T = 2$ K (circles), $T = 3$ K (squares), $T = 4$ K (diamonds) and $T = 5$ K (triangles). The arrow indicates the metamagnetic transition in the $T = 2$ K isotherm. This transition is shown magnified within the inset for clarity.

3.3. Electrical resistivity

The resistivity $\rho(T)$ is presented in figure 4. It decreases with decreasing temperature in correspondence with metallic behaviour. After correcting for the residual resistivity ρ_0 arising mainly from microcracks inherent in all polycrystalline samples, the room temperature

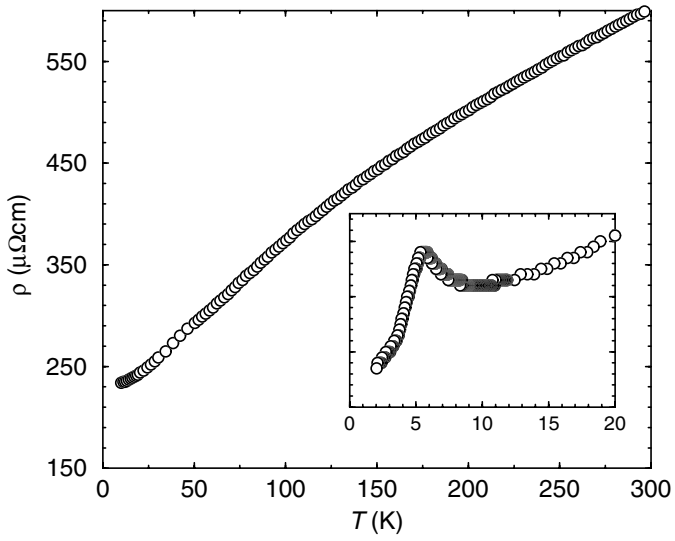

Figure 4. The temperature dependence of the resistivity $\rho(T)$ of HoAuGe. The low-temperature region within which the magnetic ordering occurs is highlighted in the inset.

resistivity is observed to be $\rho_{300\,\mathrm{K}} - \rho_0 \approx 340\ \mu\Omega$ cm. This value is large compared to those of good metals and at the upper limit of those observed for intermetallic compounds. In the case of some non-magnetic REAuGe compounds, even higher values have been observed, e.g. for LaAuGe [3]. They can be accounted for by an additional scattering mechanism arising from a narrow band near E_F as evidenced from band-structure calculations [3].

The resistivity curve below $T = 20$ K is shown magnified within the inset of figure 4. A slight upturn is observed starting at $T \approx 10$ K, and culminating in a maximum at $T = 5.5(5)$ K, corresponding closely to the previously derived value of T_N. Below this temperature, the resistivity decreases sharply, showing an additional anomaly at $T \approx 3.5$ K.

3.4. Heat capacity

The results of the heat capacity measurements are shown in figure 5. Transition peaks in the specific heat capacity $c_p(T)$ are clearly observed at temperatures of $T_N = 5.6(2)$ K, $T_1 = 3.5(2)$ K and $T_2 = 2.4(2)$ K, which correspond closely to the magnetic transitions detected in the susceptibility. Due to the high-temperature resolution of the calorimetric measurement, the peak at T_1 is seen to be composed of two closely neighbouring peaks.

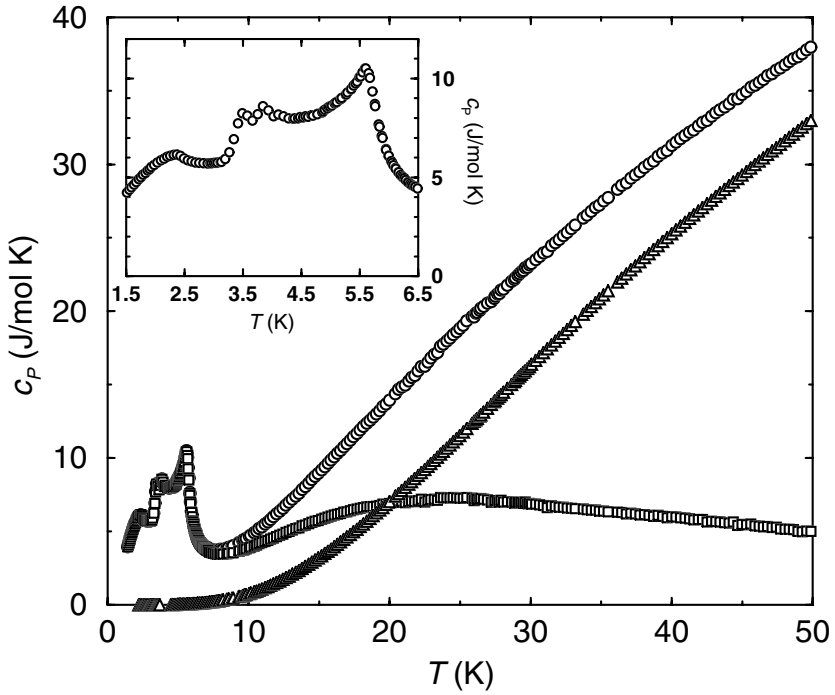

Figure 5. The heat capacity of HoAuGe. Open circles represent the measured data ($c_p(T)$), while the squares and triangles are the magnetic (c_{mag}) and (c_{latt}) lattice contributions from LuAuGe, respectively. The magnetic peaks below T_N are shown expanded within the inset for clarity.

The total heat capacity $c_p(T)$ of HoAuGe may be considered to be composed of three contributions:

$$c_p(T) = c_{\mathrm{latt}}(T) + c_{\mathrm{el}}(T) + c_{\mathrm{mag}}(T)$$

where $c_{\mathrm{latt}}(T)$ is the lattice contribution and $c_{\mathrm{el}}(T) = \gamma T$ the contribution from conduction electrons. The magnetic contribution $c_{\mathrm{mag}}(T)$ consists of two parts: a contribution $c_{4\mathrm{f}}$ arising

from magnetic effects due to the 4f electronic moments on the RE atoms and the high-temperature tail of a Schottky anomaly c_{nucl} arising from the splitting of nuclear levels. The latter term is described by $c_{\mathrm{nucl}} = aT^{-2}$. It is often negligible for measurements in the ^{4}He range, but in the case of Ho metal the contribution is anomalously large [18] and might be a significant contribution in HoAuGe at the lowest measured temperatures.

In order to separate these individual terms, the lattice and electronic contributions were derived from $c_p(T)$ for the isostructural and non-magnetic compound LuAuGe [3]. $c_{\mathrm{latt}}(T)$ for HoAuGe was calculated from $c_{\mathrm{latt}}(T)$ for LuAuGe using a method described in [3] which takes corrections for the different molar masses and lattice constants of the two compounds into account. The electronic specific heat coefficient of LuAuGe ($\gamma = 0.402$ mJ mol^{-1} K^{-2}) is rather small [3]. For intermetallic compounds with magnetic RE, γ is often an order of magnitude larger than this value; however, we have to assume the same value for γ of HoAuGe without further information on the electronic density of states at E_{F}. Any influence of a possibly enhanced γ in HoAuGe can surely be neglected for the interpretation of the magnetic contributions.

The contribution $c_{\mathrm{mag}}(T)$ obtained after subtraction of c_{latt} and c_{el} is plotted in figure 5. Without additional data on the nuclear Schottky term, e.g. c_p-measurements at lower T, a further separation of $c_{\mathrm{mag}}(T)$ is impossible.

$c_{\mathrm{mag}}(T)$ contains the peaks resulting from the magnetic ordering of the Ho ions and a superimposed Schottky anomaly above T_{N} with a broad maximum centred at $T_{\mathrm{Sch}} \approx 24$ K. Ho^{3+} is a non-Kramers ion and has a $^5I_8$ ground state. Given the symmetry of the Ho site ($3m$), a singlet ground state is allowed. Due to crystalline-electric-field (CEF) action, the ground state may split into a maximum of $2J + 1 = 17$ individual levels. The ambiguity of fitting 17 energy levels makes a meaningful fit of the Schottky anomaly impossible in the current analysis.

The magnetic entropy $S_{\mathrm{mag}}(T) = \int (c_{\mathrm{mag}}/T)\,\mathrm{d}T$ is shown in figure 6. For temperatures below the lowest measured data point (1.433 K) a T^3-extrapolation in $c_{\mathrm{mag}}(T)$ was utilized yielding $S = 0.159R$. At the foot of the magnetic ordering peak, at a temperature of 7.0 K,

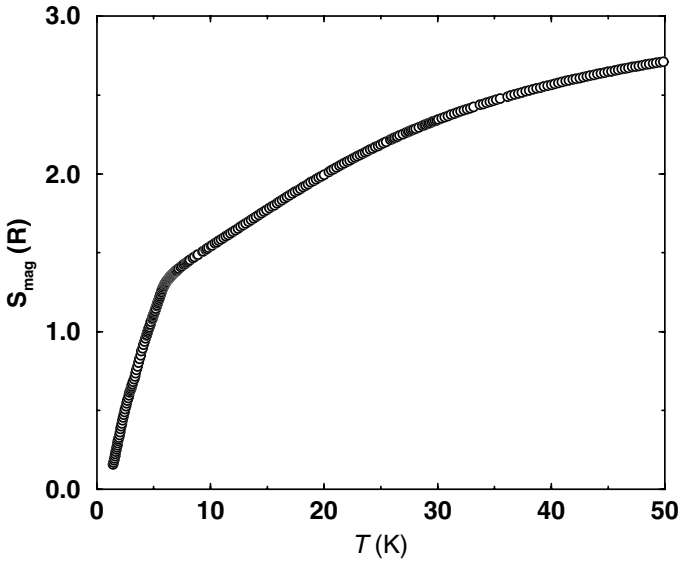

Figure 6. The temperature dependence of the magnetic entropy $S_{\mathrm{mag}}(T)$ of HoAuGe.

a magnetic entropy of about $R \ln 4$ is removed. This indicates that the magnetic ordering involves about four levels in total. Interestingly, a value of $R \ln 2$ is reached at 3.20 K—a temperature above T_2 and below T_1. Possibly, the ground state of the Ho is a doublet and another two levels are within an energy splitting of the order of T_N. The next-higher excited CEF levels, which are primarily relevant for the low-temperature rise of the Schottky anomaly, can be estimated to lie at an energy of ≈50 K.

3.5. Neutron powder diffraction

Neutron diffraction patterns were initially measured at $T = 50$ K in order to check the nuclear structure and purity of the sample, and then at the lowest temperature of $T = 1.3$ K for the determination of the magnetic structure (figure 7, top and bottom, respectively). Between these two limits, a scan in temperature was subsequently performed to follow the evolution of the magnetic structure (figure 8). The two small peaks centred around $2\theta \approx 72^\circ$ both originate from the diffractometer.

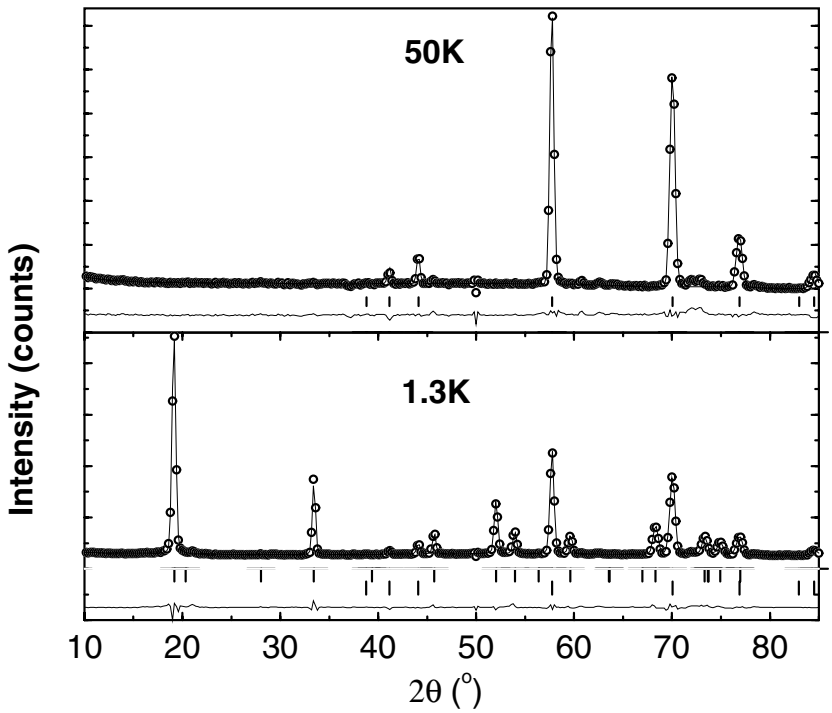

Figure 7. Neutron powder diffraction patterns of HoAuGe taken at 50 K (top) and 1.3 K (bottom). Experimental points are represented by open circles and the full line is the Rietveld fit to the data. The difference pattern and also the peak positions are shown beneath the data. The uppermost vertical bars correspond to the nuclear peaks and the lower vertical bars to the magnetic peaks.

The refinements in all cases were made using the Rietveld method [20], with the program FULLPROF [21]. Starting values for the nuclear structure determination at $T = 50$ K were obtained from the single-crystal x-ray diffraction results. From the $T = 50$ K diffraction pattern a total of eight Bragg peaks were observed, from which the scale factor (one variable), lattice parameters (two variables), pseudo-Voigt line-shape (four variables) and atomic coordinates (two variables) were refined. The final refinement converges to a Bragg R-factor of 3.6%, and

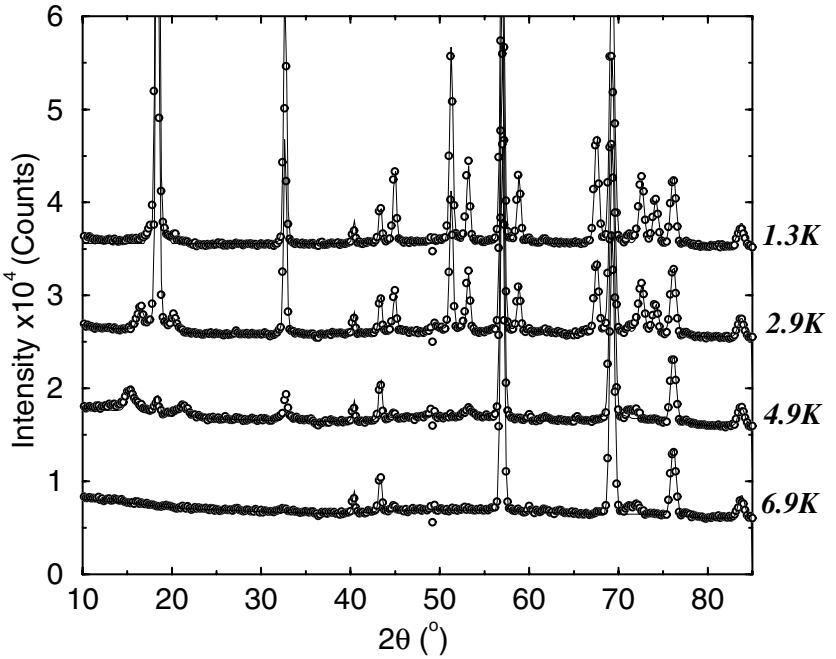

Figure 8. Neutron powder diffraction patterns of HoAuGe at the temperatures indicated. Experimental points are represented by open circles and the full lines are Rietveld fits to the data.

is in good agreement with the x-ray diffraction results, with no impurity phases evident. The lattice and atomic parameters obtained were compared with the single-crystal x-ray diffraction results in table 2. A significant contraction along the c-axis is observed with decreasing temperature. This originates in an increased puckering of the polyanion [AuGe] layers at lower temperatures.

At $T = 1.3$ K, the diffraction pattern (figure 7, bottom) displays several additional peaks which arise from coherent magnetic scattering. The magnetic peaks can be indexed on the basis of a $\vec{k} = (1/2, 0, 0)$ propagation vector. From a consideration of the allowed magnetic arrangements using the methods of representation analysis [22], four elements, β, of the space group $P6_3mc$ are observed to be invariant under the operation of the $\vec{k} = (1/2, 0, 0)$ propagation vector according to

$$\beta\vec{k} = \vec{k} + \vec{K}$$

where $\vec{K}$ is a reciprocal-lattice vector.

The four elements form a subgroup G_k of $P6_3mc$. This can be represented by four one-dimensional irreducible representations Γ_i the characters of which are listed in table 4.

Table 4. Character table showing the irreducible representations of G_k.

	E	2	m_{2xx}	c_{yz}
Γ_1	1	1	1	1
Γ_2	1	1	$\bar{1}$	$\bar{1}$
Γ_3	1	$\bar{1}$	1	$\bar{1}$
Γ_4	1	$\bar{1}$	$\bar{1}$	1

These four elements are E and m_{2xx}, which project the Ho atoms into the same positions, and 2 and c_{yz}, which shift the Ho atoms from $(0, 0, 0)$ to $(0, 0, 1/2)$. On testing each possible configuration in turn, it is found that the Γ_3 representation correctly describes the magnetic structure. This arrangement corresponds to an antiferromagnetic coupling of the Ho magnetic moments along the a-axis and ferromagnetic coupling along the b- and c-axes. The fit to the data results in a Ho magnetic moment of 6.9(1) μ_B oriented within the bc-plane. The magnetic structure is presented in figure 9 and the details of the magnetic refinement are listed in table 5.

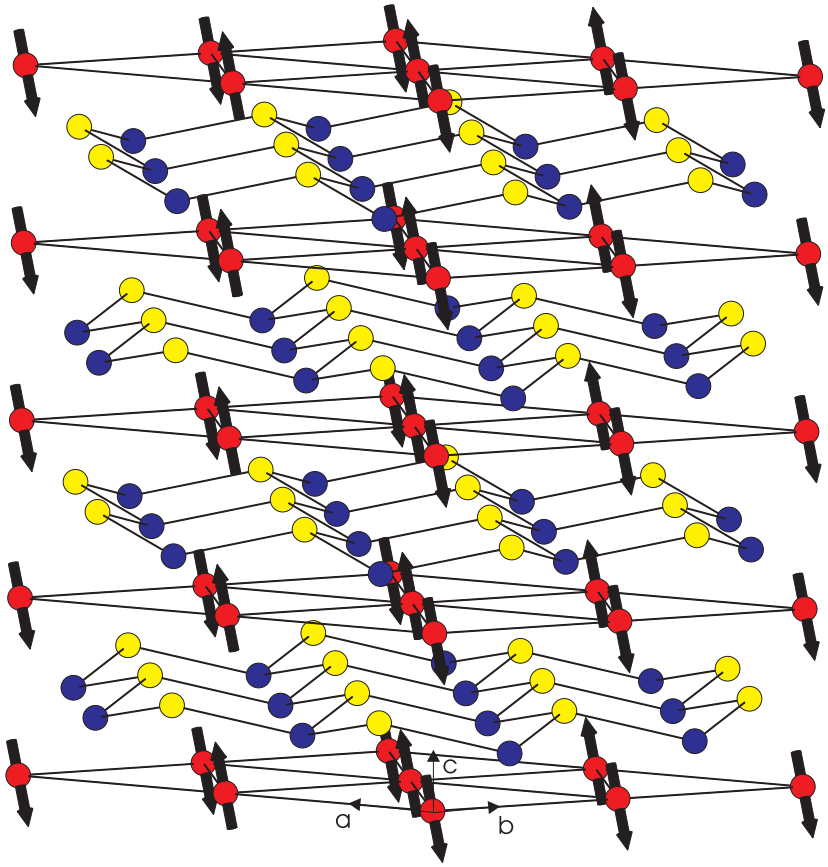

Figure 9. The magnetic structure of HoAuGe at 1.3 K. All atomic positions are shown. The arrows represent the direction and magnitude of the magnetic moments on the Ho atoms.

Two additional diffraction patterns were recorded below T_N: at $T = 2.9$ K and $T = 4.9$ K. These are shown in figure 8. As the temperature is increased towards T_N there is a gradual evolution to an incommensurate magnetic structure, as is apparent from the appearance of small satellite peaks flanking the low-angle magnetic peaks. The incommensurate structure can be indexed on the basis of two propagation vectors: $\vec{k}_1 = (1/2, 0, 0)$, corresponding to the commensurate phase already described above; and $\vec{k}_2 = (0, k_y, 0)$, upon which the satellite peaks can be indexed. $\vec{k}_y$ is observed to be temperature dependent. The result is an *amplitude-modulated* magnetic structure described as the superposition of two sine waves with amplitude m_1 and m_2 having the periodicity of $\vec{k}_1$ and $\vec{k}_2$, respectively. The magnetic structure

Table 5. Results of the magnetic Rietveld refinements of HoAuGe at $T = 1.3$ K, 2.9 K and 4.9 K. The magnetic moments $\mu_{y,\mathrm{exp}}$ and $\mu_{z,\mathrm{exp}}$ are aligned parallel to the a- and c-axis, respectively. The corresponding total experimental value μ_{exp} is compared to the theoretical value, $\mu_S = gJ\mu_B$. The magnetic moments of the two Ho sites were constrained to be equal.

T (K):	1.3		2.9		4.9	
	$\vec{k}_1$ (1/2, 0, 0)	$\vec{k}_2$ —	$\vec{k}_1$ (1/2, 0, 0)	$\vec{k}_2$ (0, 0.454, 0)	$\vec{k}_1$ (1/2, 0, 0)	$\vec{k}_2$ (0, 0.424, 0)
$\mu_{x,\mathrm{exp}}$	—	—	—	3.1(2)	—	3.2(5)
$\mu_{y,\mathrm{exp}}$	2.1(1)	—	—	—	—	–
$\mu_{z,\mathrm{exp}}$	6.5(1)	—	5.8(1)	—	1.3(4)	–
μ_{exp}	6.9(1)	6.9(1)	6.7(1)	6.7(1)	3.5(5)	3.5(5)
R_{M}	2.63	—	5.6	23.5	55.1	43.46

is incommensurate with the underlying crystal lattice and is described by the general formula

$$\vec{m}(\mathrm{Ho}) = \vec{m}_1 \exp 2\pi \mathrm{i}\vec{k}_1 \cdot \vec{r} + \vec{m}_2 \exp 2\pi \mathrm{i}\vec{k}_2 \cdot \vec{r}$$

where $\vec{m}(\mathrm{Ho})$ is the resulting magnetic moment residing on the Ho atoms, $\vec{m}_1$ and $\vec{m}_2$ are moment contributions propagating with vectors $\vec{k}_1$ and $\vec{k}_2$, respectively, and $\vec{r}$ is a lattice vector. The results of the refinements are listed in table 5 and are shown in figure 8 as the full lines passing through the measured points. The temperature evolution of the magnetic structure clearly demonstrates the change in the magnetic ordering at T_{N} and T_2. However, the change occurring at T_1 cannot be resolved due the resolution of the diffraction patterns and their temperature spacing. It is also possible that an intermediate phase occurs within the double structure of T_1 resolved in $c_p(T)$ which is only stable over a range of some 10 mK.

4. Discussion

The crystal structure of HoAuGe is derived from the $CaIn_2$-type structure [23] by an ordered arrangement of the gold and germanium atoms at the indium position. As a detailed description of the crystal chemistry of these intermetallic compounds was already given [2], the crystal structure is only briefly discussed. The gold and germanium atoms form puckered Au_3Ge_3 hexagons with intralayer Au–Ge distances of 260.5 pm, in good agreement with the sum of the Pauling single-bond radii of 255.9 pm [24] for Au and Ge. These intralayer Au–Ge interactions are of strongly bonding character, as recently shown by band-structure calculations [3]. The interlayer Au–Ge distance amounts to 304.1 pm, indicating only negligible interactions between the layers. The [AuGe] polyanion therefore has a pronounced two-dimensional character and the structure of HoAuGe may be ascribed to the NdPtSb [25] branch of the ordered $CaIn_2$ structure.

From an examination of the magnetic properties of HoAuGe, we observe a good agreement with the Curie–Weiss law at temperatures sufficiently higher than T_{N}. The small value of the paramagnetic Curie constant ($\Theta_{\mathrm{p}} = 0(1)$ K), coupled with the large interatomic spacing between Ho ions, indicates that either the antiferromagnetic and ferromagnetic exchange interactions are very small or they cancel out almost equally within HoAuGe.

The antiferromagnetic transition is found to occur at $T_{\mathrm{N}} = 5.6(2)$ K as is evident from heat capacity and susceptibility measurements. In that context it is interesting to note that a scaling of magnetic transition temperatures with the de Gennes factor is not found for the several REAuGe compounds investigated by our group up to now [26]. In addition, two further transitions are found below T_{N} at $T_1 = 3.5(2)$ K and $T_2 = 2.4(2)$ K. A recent paper by Penc

et al [27] has also reported susceptibility measurements of several REAuGe compounds. In particular they calculate values of $T_N = 7.6$ K, $\Theta_p = -5.1$ K, $\mu_{eff}^{exp} = 10.1\ \mu_B$ and a high-field saturation magnetic moment of 6.9 μ_B/Ho atom for HoAuGe, and also make no mention of the anomalies below T_N. These results are significantly different from those presented within this paper. A possible explanation for this difference could be the sample preparation. It is conceivable that, under different annealing conditions, the Au and Ge atoms within the [AuGe] polyanionic layers form a random distribution, resulting in a different Ho^{3+} CEF environment, and hence different magnetic properties. However, this cannot be proven as no crystallographic details are mentioned in their paper [27].

The observed magnetic transitions below T_N are explained in terms of changes in the magnetic structure which are revealed by the neutron diffraction experiments. At 4.9 K, just below T_N, the magnetic structure is incommensurate with the crystal lattice and can be described as the superposition of components of the Ho magnetic moments propagating with two different wave vectors. The magnetic structure changes gradually as the temperature is lowered as observed from an increase in k_2 and an increase of the net Ho moment until a simple commensurate structure is achieved at 1.3 K.

The tendency of a magnetic structure to change towards a simple commensurate structure as $T \rightarrow 0$ K has been previously found in several other intermetallic compounds [28]. A theoretical model has been proposed by Gignoux and Schmitt [28], who show that, on the basis of free-energy considerations, only simple commensurate magnetic structures are stable at 0 K, with incommensurate structures being more favourable at higher temperatures. Interestingly, the theory is also relevant for the application of external magnetic fields and predicts the same change towards incommensurability as the field strength is increased (up to the saturated ferromagnetic state that is always achieved if the field is strong enough). Therefore, the magnetic transition observed at 0.4 T in the 2 K isotherm of figure 3 could well indicate a change in the magnetic structure equivalent to the resolved temperature-dependent incommensurate structure.

The evolution of the magnetic entropy with temperature shows clearly that the magnetic ground state contains four levels in total. The next-higher excited levels lie at an energy of $\approx$50 K. In order to obtain more definite information about the CEF splitting, an analysis utilizing inelastic neutron scattering is desirable.

Acknowledgments

We are indebted to Dipl-Ing U Rodewald for the data collection at the x-ray four-circle diffractometer, to W Röthenbach for taking the Guinier powder patterns, to N Rollbühler for the resistivity measurements, to E Brücher for the susceptibility measurements and to Dr W Gerhartz (Degussa AG) for a generous gift of gold wire.

References

[1] Pöttgen R, Borrmann H and Kremer R K 1996 *J. Magn. Magn. Mater.* **152** 196–200
[2] Pöttgen R, Borrmann H, Felser C, Jepsen O, Henn R, Kremer R K and Simon A 1996 *J. Alloys Compounds* **235** 170–5
[3] Schnelle W, Pöttgen R, Kremer R K, Gmelin E and Jepsen O 1997 *J. Phys.: Condens. Matter* **9** 1435–50
[4] Gibson B J, Schnelle W, Pöttgen R, Bartkowski K and Kremer R K 1996 *Czech. J. Phys.* **46** 2573–4
[5] Gibson B J 1998 Investigation of the physical properties of the ternary rare-earth intermetallic compounds, RETGe (RE = Sc, Y, La–Lu; T = Ag, Au) *PhD Thesis* Loughborough University, UK
[6] Pöttgen R 1995 *J. Mater. Chem.* **5** 505–8
[7] Müllmann R, Mosel B D, Eckert H, Pöttgen R and Kremer R K 1997 *Hyperfine Interact.* **108** 389–400

[8] Szytuła A and Leciejewicz J 1994 *Handbook of Crystal Structures and Magnetic Properties of Rare-Earth Intermetallics* (Boca Raton, FL: Chemical Rubber Company Press)
[9] Gibson B J, Kremer R K, Schnelle W, Ouladdiaf B and Pöttgen R 1996 *Czech. J. Phys.* **46** 2114–5
[10] Krauss H L and Stach H 1969 *Z. Anorg. Allg. Chem.* **366** 34–42
[11] Pöttgen R, Gulden Th and Simon A 1999 *GIT Labor-Fachzeitschrift* **43** 133–6
[12] Simon A 1970 *J. Appl. Crystallogr.* **3** 11–21
[13] Yvon K, Jeitschko W and Parthe E 1977 *J. Appl. Crystallogr.* **10** 73–4
[14] Rossi D, Marazza R and Ferro R 1992 *J. Alloys Compounds* **187** 267–70
[15] Gmelin E 1987 *Thermochim. Acta* **110** 183
[16] For a list of instrument characteristics see, e.g., http://www.ill.fr/YellowBook/D1B/
[17] Sheldrick G M 1993 *SHELXL-93, Program for Crystal Structure Refinement* University of Göttingen, Germany
[18] Sundström L J 1978 *Handbook on the Physics and Chemistry of Rare Earths* vol 1, ed K A Gschneidner Jr and L Eyring (Amsterdam: North-Holland) ch 5, pp 379–410
[19] Due to the small number of parameters, an automatic restraint of the floating origin is not possible; Schwarzenbach D, private communication (Lausanne)
[20] Rietveld H M 1969 *J. Appl. Crystallogr.* **2** 65–71
[21] Rodriguez-Carvajal J 1994 *FULLPROF: a Program for Rietveld Refinement and Profile Matching Analysis of Complex Powder Diffraction Patterns* Institut Laue–Langevin, France, unpublished
[22] Bertaut E F 1968 *Acta Crystallogr.* A **24** 217–31
[23] Iandelli A 1964 *Z. Anorg. Allg. Chem.* **330** 221–32
[24] Pauling L 1973 *Die Natur der Chemischen Bindung* (Weinheim: Chemie) p 245
[25] Wenski G and Mewis A 1986 *Z. Kristallogr.* **176** 125–34
[26] Schnelle W, Kremer R K, Pöttgen R and Gibson B J 1998 unpublished
[27] Penc B, Baran S, Slaski M and Szytuła A 1999 *J. Alloys Compounds* **282** L6–8
[28] Gignoux D and Schmitt D 1993 *Phys. Rev.* B **48** 12 682–91